SCIENCE CHINA
Information Sciences

• RESEARCH PAPER •

February 2024, Vol. 67, Iss. 2, 122301:1–122301:20
https://doi.org/10.1007/s11432-023-3788-y

Multi-stream signals separation based on space-time-isomeric (SPATIO) array using metasurface antennas

Yangming LOU[1], Liang JIN[1*], Huiming WANG[2], Zhou ZHONG[1] & Junyan DAI[3]

[1] *PLA Strategic Support Force Information Engineering University, Zhengzhou* 450001*, China;*
[2] *School of Information and Communications Engineering, Xi'an Jiaotong University, Xi'an* 710049*, China;*
[3] *State Key Laboratory of Millimeter Waves, Southeast University, Nanjing* 210096*, China*

Received 7 February 2023/Revised 4 May 2023/Accepted 31 May 2023/Published online 25 January 2024

Abstract In spatial domain signal processing, it is necessary to equip more antennas at the receiver to improve spatial demultiplexing capability. However, increasing the number of antennas under restricted space will reduce antenna spacing and raise the channel correlation, making the number of signal streams spatially demultiplexed much smaller than that of antennas. This paper proposes a method to design a space-time-isomeric (SPATIO) array based on metasurface antennas under wireless multipath conditions. Each antenna in this array has a different pattern and varies independently with time, reducing the channel correlation by superposing multipath at distinct positions and moments. Based on the SPATIO array, we present an array parameter design scheme based on infinity norm minimization, which can maximize the received energy of each stream while separating multi-stream received signals. Simulation results illustrate the performance of the SPATIO array for multi-stream signal reception. Compared with conventional multiple-input multiple-output arrays, the proposed array can reduce the bit error rate by one order of magnitude under the same simulation conditions.

Keywords multiple-input multiple-output, metasurface antenna, space-time-isomeric array, multipath channel, degree of freedom

1 Introduction

The rapid development of wireless communication technology continues to influence our daily life. From traditional communication services like simple daily calling and short message services to emerging information services such as streaming media, telecommuting, and telemedicine, wireless communication businesses have become abundant due to the increased communication rate. In the history of wireless communication, the improvement of communication rate has become the backbone of every technological revolution, which relies on the effective utilization of communication resources [1]. Nowadays, the high-quality spectrum resources within sub-6G are almost exhausted, and new spectrum resources can only be obtained from high-frequency bands such as millimeter waves and terahertz. However, the high operating bands increase propagation attenuation and make it challenging to apply wireless communication.

People have started exploiting spatial resources for the future vision of the "Internet of Everything". Equipping transceivers with multiple antennas increases communication capacity by utilizing the multiple-input multiple-output (MIMO) technology. Since the spatial and time-frequency resources are independent, they can realize multi-cell and multi-user communication under co-frequency co-time conditions [2]. However, with the increasing number of antennas, the channel capacity and the array degrees of freedom (DOF) do not continue to increase as expected. In general, the array DOF is equal to the number of receiving antennas, representing the maximum number of spatially multiplexed/demultiplexed signal streams the array can achieve. Currently, the number of antennas in 5G massive MIMO (mMIMO) technology is nearly several hundred, while the number of antennas in the 6G super-scale antenna technology under study is over one thousand. However, the number of signal streams, namely the effective DOF, which

* Corresponding author (email: liangjin@263.net)

can be received simultaneously in these systems is much smaller than that of antennas equipped [3–5]. Typically, an mMIMO base station with 128 antennas can serve only 10 to 20 users, which is attributed to the correlation improvement between channels due to the reduced antenna spacing. Current studies show that antenna spacing needs at least half of the wavelength to ensure channel independence even in a multipath uniform scattering environment. In engineering practice, larger spacing is required to achieve the effect [6, 7]. When the space is limited, increasing the number of antennas will only make the channel correlation grow, so this kind of crude performance enhancement mode relying on enlarging the array scale is not sustainable. On the other hand, from the engineering perspective, increasing the array scale raises both the cost and complexity.

As the broadcast of electromagnetic waves, the wireless signal will experience multiple paths of propagation. Therefore, the channel sensed by the antenna is the superposition of multiple paths, and the independence between channels also results from the independence of paths arriving at different antennas. The antenna has different amplitude and phase responses for various wave directions, which is reflected in the pattern. Once paths arrive at the antenna, they are weighted and superposed under the effect of the pattern. Conventional antenna arrays are usually isomorphic arrays, which means that the antennas in the array have fixed and identical structures with the same pattern regardless of their positions, resulting in channel differences only when the paths differ at different antennas. In far-field conditions, the path only has phase differences when reaching each antenna and gradually disappears as the antennas get closer, resulting in channel correlation. Hence, the state of arriving paths and how the paths are superposed determine the channels observed by the antennas. If the pattern of the antennas in the array can be changed independently, it is possible to adjust the way paths superpose at each antenna. So the channel difference can be enlarged even if the multipath arriving at different antennas tends to be the same. In contrast to the classical isomorphic array, we refer to these types of arrays as isomeric arrays, in which different antenna has a different pattern.

Reconfigurable antennas use internally embedded radio-frequency microelectromechanical system (RF-MEMS) switches [8–10], positive-intrinsic-negative (PIN) diodes [11, 12], varactors [13, 14], and other reconfigurable devices to change their electromagnetic characteristics and adjust the operating frequency, polarization mode, radiation pattern, to achieve different system requirements [15, 16]. Pattern reconfigurable antennas are realized by designing flexible structures or feed networks, which can be widely used in monitoring, tracking, and other fields [17]. For example, a planar pattern reconfigurable antenna proposed in [18] achieves four-directional pattern rotation by switching the on/off state of the embedded PIN diodes. Ref. [11] proposed a hybrid beam scanning and switching array based on reconfigurable antennas that can be used in 5G terminals and achieve the same spatial coverage with two-thirds of the number as compared to conventional beam scanning systems. Ref. [19], on the other hand, proposed a millimeter-wave reconfigurable antenna application scheme called reconfigurable antenna multiple access (RAMA) at the base station to realize multi-user access. In this system, the base station controls the reconfigurable antennas to form directional beams to users in different directions. It achieves multi-access by switching the beam alignment to different users. Ref. [20] demonstrated the beam forming capability of reconfigurable antenna arrays. By adjusting each antenna's pattern, the array's gain other than the normal direction can be effectively improved while reducing grating lobes.

However, reconfigurable antennas usually aim to improve the range and accuracy of beam scanning in conventional array designs, mainly for scenarios with one strong path. We must redesign the reconfigurable antennas and array for optimal multipath merging. With the recent development of metamaterial technology, research on reconfigurable metamaterial antennas has emerged. These metamaterial-based reconfigurable antennas, such as metasurface antennas [21–23], are composed of a mass of subwavelength or deep subwavelength metamaterial elements. They can rapidly change the pattern by adjusting the state of each element, thus offering a very high DOF [24–28]. This capability provides a foundation for us to use the reconfigurable pattern to change the multipath merging method and thus reduce the correlation of channels between different antennas and improve the spatial demultiplexing capability.

The authors' team has already explored the concept and basic capabilities of space-time-isomeric (SPATIO) arrays in the early stage [29]. This paper will further develop our previous research and propose a design method for the SPATIO array based on metasurface antennas. Unlike the existing isomorphic array, the SPATIO array utilizes the pattern reconfigurability of the metasurface antenna to dynamically adjust the multipath superposition method. This reduces the correlation of channels and ensures that the effective DOF is the same as the array DOF.

The contributions of this paper are summarized as follows:

• We establish a reconfigurable metasurface antenna model for wireless multipath. We propose the correspondence between the element state and the pattern with the determined layout of metamaterial elements for each antenna. Unlike existing antennas designed for directional beams, we design antenna patterns to superpose multipath optimally. The effective DOF is improved by changing the superposition of the multipath. Such a reconfigurable antenna is the prerequisite to achieving array reconfigurability.

• We propose an isomeric array design method in the spatial dimension. By adjusting the pattern of each antenna in the array, we reduce the correlation between channels on each antenna so that the effective DOF can be the same as the array DOF, which can solve the degradation of spatial demultiplexing ability due to the lack of rank for the channel matrix.

• We propose an isomeric array design method in the temporal dimension. The patterns of the metasurface antenna rapidly switch within a single symbol period. So that the single signal stream equivalently experiences different channels and becomes a virtual antenna array, which increases the effective DOF, improves the rank of the channel matrix, and enhances the spatial demultiplexing capability of the array.

• We propose a SPATIO array based on the above two according to the independence of spatial and temporal dimensions. Then, we present a multi-stream signal reception scheme based on infinity norm minimization (INM) for this array to achieve the optimal reception of each stream while ensuring the separation of received signals.

The rest of the paper is organized as follows. Section 2 introduces the metasurface antenna model and the multipath channel model. In Section 3, we show the analysis of the channel model for the space-isomeric array, time-isomeric array, and SPATIO array, then propose an array design method based on INM. The performance analysis of the SPATIO array is presented in Section 4 as numerical simulations. At last, the paper is summarized in Section 5.

Notations. A bold lowercase $\boldsymbol{a}$ denotes the column vector, a bold capital letter $\boldsymbol{A}$ denotes the matrix, $(\cdot)^{\mathrm{T}}$ and $(\cdot)^{\mathrm{H}}$ denote the transpose and Hermitian transpose, respectively. $\mathrm{rank}(\cdot)$ means the rank of matrix, $\|\cdot\|_2$ and $\|\cdot\|_\infty$ denote l_2-norm and l_∞-norm, respectively. $\mathbb{C}$ denotes complex field.

2 Metasurface antenna model for multipath signal reception

2.1 Metasurface antenna

A metasurface antenna is a planar antenna consisting of several compact spaced metamaterial elements. Figure 1 shows an example of a metasurface antenna consisting of a square of metamaterial elements. Each metamaterial element is controlled by an electronic switching component, such as PIN diodes or varactors, enabling it to adjust the amplitude, phase, and other parameters of electromagnetic signals.

To describe the response of the metasurface antenna more conveniently, we establish the following Cartesian coordinate system as Figure 1. Let O^{ϕ} be the phase reference center of the metasurface antenna. For each metamaterial element i, there is a vector $\boldsymbol{q}_i$ pointing from O^{ϕ} to the metamaterial element i. Denote a unit vector $\boldsymbol{e}_l$ as the incidence direction of the signal with $|\boldsymbol{e}_l| = 1$. The angle between $\boldsymbol{e}_l$ and the normal direction of the metamaterial element is θ. Then relative to the phase reference center O^{ϕ}, the phase of the far-field signal arrived at the metamaterial element i is

$$\epsilon_i = \frac{2\pi|\boldsymbol{q}_i|\sin\theta}{\lambda} = \frac{2\pi\langle \boldsymbol{q}_i, \boldsymbol{e}_l\rangle}{\lambda}, \tag{1}$$

where λ is the carrier wavelength, $|\cdot|$ denotes the length of vector, $\langle \boldsymbol{q}_i, \boldsymbol{e}_l\rangle$ denotes the projection length of $\boldsymbol{q}_i$ on $\boldsymbol{e}_l$, and the second equality comes from

$$|\boldsymbol{q}_i|\sin\theta = |\boldsymbol{q}_i||\boldsymbol{e}_l|\cos\gamma = \langle \boldsymbol{q}_i, \boldsymbol{e}_l\rangle. \tag{2}$$

In the Cartesian coordinate system $\langle \boldsymbol{q}_i, \boldsymbol{e}_l\rangle = \boldsymbol{q}_i^{\mathrm{T}}\boldsymbol{e}_l$, then

$$\epsilon_i = \frac{2\pi\boldsymbol{q}_i^{\mathrm{T}}\boldsymbol{e}_l}{\lambda}. \tag{3}$$

Due to the small size of the metamaterial element, the directionality of individual element response is weak, and the response of each metamaterial element can be approximated as a uniform attenuation and phase shift of the signals arriving in all directions, which is denoted as a complex coefficient w_i.

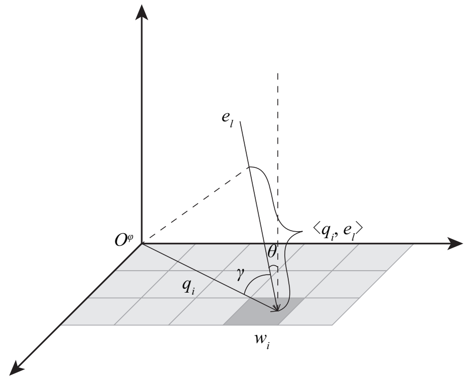

Figure 1 Structure of the metasurface antenna is planar, which consists of compact spaced metamaterial elements.

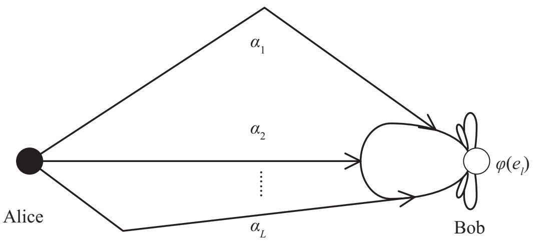

Figure 2 Pattern can influence the superposition of multipath for any receive antenna.

Assuming that the metasurface antenna consists of I elements, the response of the metasurface antenna to a signal coming from direction $\boldsymbol{e}_l$, which is called the pattern, can be written as

$$\phi(\boldsymbol{e}_l) = \sum_{i=1}^{I} w_i \mathrm{e}^{\frac{-\mathrm{j}2\pi \boldsymbol{q}_i^{\mathrm{T}} \boldsymbol{e}_l}{\lambda}}. \tag{4}$$

Since the coefficients $w_i, i = 1, 2, \ldots, I$ can be controlled flexibly, the response of the metasurface antenna is also adjustable. This is a significant feature of the metasurface antenna. According to (4), we can see that for any signal coming from direction $\boldsymbol{e}_i$, the response is determined by the structure of the antenna $\boldsymbol{q}_i$, and the coefficients $w_i, i = 1, 2, \ldots, I$.

2.2 Response of metasurface antenna in multipath flat fading channel

As shown in Figure 2, the transmitted signals reach the receiver through multipath. Assuming that paths are coming from directions $\boldsymbol{e}_1, \ldots, \boldsymbol{e}_L$, according to (4), the response of the multipath signals can be rewritten in matrix form as

$$\begin{bmatrix} \phi(\boldsymbol{e}_1) \\ \vdots \\ \phi(\boldsymbol{e}_L) \end{bmatrix} = \boldsymbol{A}_{[\boldsymbol{E}^{\mathrm{T}}\boldsymbol{Q}]} \boldsymbol{w}, \tag{5}$$

where

$$\boldsymbol{A}_{[\boldsymbol{E}^{\mathrm{T}}\boldsymbol{Q}]} = \begin{bmatrix} \mathrm{e}^{\frac{-\mathrm{j}2\pi \boldsymbol{e}_1^{\mathrm{T}} \boldsymbol{q}_1}{\lambda}} & \cdots & \mathrm{e}^{\frac{-\mathrm{j}2\pi \boldsymbol{e}_1^{\mathrm{T}} \boldsymbol{q}_I}{\lambda}} \\ \vdots & \ddots & \vdots \\ \mathrm{e}^{\frac{-\mathrm{j}2\pi \boldsymbol{e}_L^{\mathrm{T}} \boldsymbol{q}_1}{\lambda}} & \cdots & \mathrm{e}^{\frac{-\mathrm{j}2\pi \boldsymbol{e}_L^{\mathrm{T}} \boldsymbol{q}_I}{\lambda}} \end{bmatrix}, \tag{6}$$

and $\boldsymbol{Q} = [\boldsymbol{q}_1, \ldots, \boldsymbol{q}_I]$, $\boldsymbol{E} = [\boldsymbol{e}_1, \ldots, \boldsymbol{e}_L]$, and $\boldsymbol{w} = [w_1, \ldots, w_I]^{\mathrm{T}}$. $\boldsymbol{Q}$ is determined by the structure of the antenna, $\boldsymbol{E}$ could be called the direction matrix which depends on the propagation channel, and $\boldsymbol{w}$ is the adjustable parameters based on the reconfigurable capability of the metasurface antenna.

For a signal x that goes through the above flat fading channel with the complex gain of path l as α_l, the received signal y at the metasurface antenna can be expressed as

$$y = \sum_l \phi(\boldsymbol{e}_l)\alpha_l x + z = \begin{bmatrix} \phi(\boldsymbol{e}_1) & \cdots & \phi(\boldsymbol{e}_L) \end{bmatrix} \begin{bmatrix} \alpha_1 \\ \vdots \\ \alpha_L \end{bmatrix} x + z = \boldsymbol{\phi}^{\mathrm{T}} \boldsymbol{\alpha} x + z. \tag{7}$$

where z denotes the noise. x reaches the metasurface antenna through the multipath channel $\boldsymbol{\alpha}$ from different directions $\boldsymbol{e}_1, \ldots, \boldsymbol{e}_L$, which activate different responses and enters the receiver channel after weighted superposition. The equivalent overall channel becomes $\boldsymbol{\phi}^{\mathrm{T}}\boldsymbol{\alpha}$.

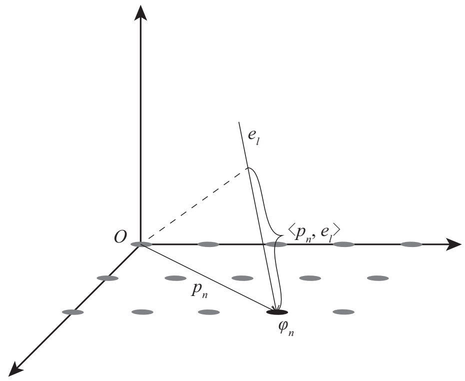

Figure 3 In the space-isomeric array, antennas at different locations have distinct patterns.

Obviously, it is possible to change the equivalent channel by adjusting the pattern $\boldsymbol{\phi}$. We put (5) into (7), then

$$y = (\boldsymbol{A}_{[\boldsymbol{E}^{\mathrm{T}}\boldsymbol{Q}]}\boldsymbol{w})^{\mathrm{T}}\boldsymbol{\alpha}x + z = \boldsymbol{w}^{\mathrm{T}}\boldsymbol{A}_{[\boldsymbol{Q}^{\mathrm{T}}\boldsymbol{E}]}\boldsymbol{\alpha}x + z. \tag{8}$$

We can see that compared with a conventional antenna, which has a fixed pattern determined by the material and geometry structure, a metasurface antenna can change $\boldsymbol{w}$ flexibly, so that $\boldsymbol{\phi}$ can change the multipath superposition and thus affect y by designing $\boldsymbol{w}$ for $\boldsymbol{A}$. Similarly, the results can also be extended to other types of reconfigurable antennas by finding a mapping relationship between configuration parameters and antenna patterns as described in (5).

It should be noted that for narrowband signals, the time delay is equivalent to the phase difference, in which case the frequency selective fading channel is identical to the flat fading channel. However, for wideband signals, the received signal model in (7) will no longer be applicable since the pattern is frequency dependent. Fortunately, most commercial communication systems employ narrowband signals or can split broadband signals into narrowband signals, such as OFDM systems, and the model still holds for each subband. Therefore, we focus our study mainly on flat fading channel.

3 SPATIO array design

With the above model of metasurface antenna, in this section, we introduce our proposed SPATIO array. In the following, we first introduce the space-isomeric array and time-isomeric array, respectively. The SPATIO array can be considered as the combination of these two.

3.1 Space-isomeric array

A space-isomeric array is an antenna array where each array element is a metasurface antenna. We call it a space-isomeric array because each element may have a different pattern while in conventional antenna arrays, they have the same pattern. With the capability of pattern adjustment, antennas at different locations can adjust their pattern according to the channel multipath to achieve better performance. In this subsection, we analyze the DOF of the space-isomeric array, which has a critical impact on the channel capacity. Without loss of generality, we discuss the case of the uniform plane array.

The uniform plane array is shown in Figure 3, where each element is a square metasurface antenna shown in Figure 1, and the total number of antennas is N. Let O denote the array phase center, $\boldsymbol{p}_n$ is the vector pointing from O to the phase center of the metasurface antenna n, and ϕ_n denotes the pattern of antenna n. $\langle \boldsymbol{p}_n, \boldsymbol{e}_l\rangle$ denotes the inner product of $\boldsymbol{p}_n$ and $\boldsymbol{e}_l$, $\langle \boldsymbol{p}_n, \boldsymbol{e}_l\rangle = \boldsymbol{p}_n^{\mathrm{T}}\boldsymbol{e}_l$.

Assuming there are M sources, and $N \geqslant M$. For each source m, there are L_m paths with incoming directions $\boldsymbol{e}_{ml}$ and fading coefficients $\alpha_{ml}, l = 1, 2, \ldots, L_m$ at O. Then the pattern of the n-th antenna is $\phi_n(\boldsymbol{e}_{ml})$. In the far-field condition, the received signal of antenna n is

$$y_n = \sum_{m=1}^{M}\sum_{l=1}^{L_m}\phi_n(\boldsymbol{e}_{ml})\mathrm{e}^{\frac{-\mathrm{j}2\pi\boldsymbol{p}_n^{\mathrm{T}}\boldsymbol{e}_{ml}}{\lambda}}\alpha_{ml}x_m + z_n, \tag{9}$$

where x_m denotes the transmitted signal from the source m and z_n is the received noise at antenna n. Inserting (4) into (9) yields

$$\begin{aligned} y_n &= \sum_{m=1}^{M} x_m \sum_{l=1}^{L_m} \sum_{i=1}^{I} w_{ni} \mathrm{e}^{\frac{-\mathrm{j}2\pi \boldsymbol{q}_i^{\mathrm{T}} \boldsymbol{e}_{ml}}{\lambda}} \mathrm{e}^{\frac{-\mathrm{j}2\pi \boldsymbol{p}_n^{\mathrm{T}} \boldsymbol{e}_{ml}}{\lambda}} \alpha_{ml} + z_n \\ &= \sum_{m=1}^{M} x_m \sum_{l=1}^{L_m} \sum_{i=1}^{I} w_{ni} \mathrm{e}^{\frac{-\mathrm{j}2\pi (\boldsymbol{p}_n+\boldsymbol{q}_i)^{\mathrm{T}} \boldsymbol{e}_{ml}}{\lambda}} \alpha_{ml} + z_n, \end{aligned} \tag{10}$$

which can be expressed in a matrix form as

$$\begin{bmatrix} y_1 \\ \vdots \\ y_N \end{bmatrix} = \begin{bmatrix} \boldsymbol{w}_1^{\mathrm{T}} \boldsymbol{A}_{[(\boldsymbol{P}_1+\boldsymbol{Q})^{\mathrm{T}}\boldsymbol{E}_1]} \boldsymbol{\alpha}_1 & \cdots & \boldsymbol{w}_1^{\mathrm{T}} \boldsymbol{A}_{[(\boldsymbol{P}_1+\boldsymbol{Q})^{\mathrm{T}}\boldsymbol{E}_M]} \boldsymbol{\alpha}_M \\ \vdots & \ddots & \vdots \\ \boldsymbol{w}_N^{\mathrm{T}} \boldsymbol{A}_{[(\boldsymbol{P}_N+\boldsymbol{Q})^{\mathrm{T}}\boldsymbol{E}_1]} \boldsymbol{\alpha}_1 & \cdots & \boldsymbol{w}_N^{\mathrm{T}} \boldsymbol{A}_{[(\boldsymbol{P}_N+\boldsymbol{Q})^{\mathrm{T}}\boldsymbol{E}_M]} \boldsymbol{\alpha}_M \end{bmatrix} \begin{bmatrix} x_1 \\ \vdots \\ x_M \end{bmatrix} + \begin{bmatrix} z_1 \\ \vdots \\ z_N \end{bmatrix}, \tag{11}$$

where

$$\boldsymbol{A}_{[(\boldsymbol{P}_n+\boldsymbol{Q})^{\mathrm{T}}\boldsymbol{E}_m]} = \begin{bmatrix} \mathrm{e}^{\frac{-\mathrm{j}2\pi \boldsymbol{e}_1^{\mathrm{T}}(\boldsymbol{p}_n+\boldsymbol{q}_1)}{\lambda}} & \cdots & \mathrm{e}^{\frac{-\mathrm{j}2\pi \boldsymbol{e}_1^{\mathrm{T}}(\boldsymbol{p}_n+\boldsymbol{q}_I)}{\lambda}} \\ \vdots & \ddots & \vdots \\ \mathrm{e}^{\frac{-\mathrm{j}2\pi \boldsymbol{e}_L^{\mathrm{T}}(\boldsymbol{p}_n+\boldsymbol{q}_1)}{\lambda}} & \cdots & \mathrm{e}^{\frac{-\mathrm{j}2\pi \boldsymbol{e}_L^{\mathrm{T}}(\boldsymbol{p}_n+\boldsymbol{q}_I)}{\lambda}} \end{bmatrix}, \tag{12}$$

$\boldsymbol{w}_n = [w_{n1}, \ldots, w_{nI}]^{\mathrm{T}}$, $\boldsymbol{\alpha}_m = [\alpha_{m1}, \ldots, \alpha_{mL_m}]^{\mathrm{T}}$, $\boldsymbol{P}_n = [\boldsymbol{p}_n, \ldots, \boldsymbol{p}_n]$, and $\boldsymbol{Q} = [\boldsymbol{q}_1, \ldots, \boldsymbol{q}_I]$.

Let $\boldsymbol{B}_n \triangleq [\boldsymbol{A}_{[(\boldsymbol{P}_n+\boldsymbol{Q})^{\mathrm{T}}\boldsymbol{E}_1]}\boldsymbol{\alpha}_1, \ldots, \boldsymbol{A}_{[(\boldsymbol{P}_n+\boldsymbol{Q})^{\mathrm{T}}\boldsymbol{E}_M]}\boldsymbol{\alpha}_M]$, then Eq. (11) can be written as

$$\boldsymbol{y} = \boldsymbol{H}\boldsymbol{x} + \boldsymbol{z}, \tag{13}$$

where $\boldsymbol{y} = [y_1, \ldots, y_N]^{\mathrm{T}}$, $\boldsymbol{x} = [x_1, \ldots, x_M]^{\mathrm{T}}$, $\boldsymbol{z} = [z_1, \ldots, z_N]^{\mathrm{T}}$, and

$$\boldsymbol{H} = \begin{bmatrix} \boldsymbol{w}_1^{\mathrm{T}} & & \\ & \ddots & \\ & & \boldsymbol{w}_N^{\mathrm{T}} \end{bmatrix} \begin{bmatrix} \boldsymbol{B}_1 \\ \vdots \\ \boldsymbol{B}_N \end{bmatrix}. \tag{14}$$

This is an equivalent MIMO channel. It can be seen from (11) that, in contrast to the classical MIMO channel model, the channel matrix of the space-isomeric array is jointly defined by the antenna configuration parameters $\boldsymbol{w}_1, \ldots, \boldsymbol{w}_N$ and the multipath channel matrix $[\boldsymbol{B}_1^{\mathrm{T}}, \ldots, \boldsymbol{B}_N^{\mathrm{T}}]^{\mathrm{T}}$. The rank of the channel matrix determines the number of signal streams an array can separate, which is affected by $\boldsymbol{w}_n$. We have Theorem 1.

Theorem 1. For a space-isomeric array with array DOF of N, as long as the rank of the multipath channel matrix is N, the spatial demultiplexing of N-stream signals can be achieved, i.e., the effective DOF is N, even if the channels between antennas are strongly correlated.

Proof. When the antenna spacing is 0, the Pearson correlation coefficient between channels is 1, which means that the correlation is strongest at this time, so we prove the theorem under this condition. Let all antennas be located at the coordinate origin O. At this point $\boldsymbol{P} \triangleq \boldsymbol{P}_1 = \cdots = \boldsymbol{P}_N$, and the elements in $\boldsymbol{P}$ are all 0, Eq. (11) can be written in the following form:

$$\begin{bmatrix} y_1 \\ \vdots \\ y_N \end{bmatrix} = \begin{bmatrix} \boldsymbol{w}_1^{\mathrm{T}} \\ \vdots \\ \boldsymbol{w}_N^{\mathrm{T}} \end{bmatrix} \begin{bmatrix} \boldsymbol{A}_{[\boldsymbol{Q}^{\mathrm{T}}\boldsymbol{E}_1]}\boldsymbol{\alpha}_1 & \cdots & \boldsymbol{A}_{[\boldsymbol{Q}^{\mathrm{T}}\boldsymbol{E}_M]}\boldsymbol{\alpha}_M \end{bmatrix} \begin{bmatrix} x_1 \\ \vdots \\ x_M \end{bmatrix} + \begin{bmatrix} z_1 \\ \vdots \\ z_N \end{bmatrix}, \tag{15}$$

denote

$$\begin{aligned} \boldsymbol{W} &\triangleq [\boldsymbol{w}_1, \ldots, \boldsymbol{w}_N]_{I\times N}, \\ \boldsymbol{B} &\triangleq [\boldsymbol{A}_{[\boldsymbol{Q}^{\mathrm{T}}\boldsymbol{E}_1]}\boldsymbol{\alpha}_1, \ldots, \boldsymbol{A}_{[\boldsymbol{Q}^{\mathrm{T}}\boldsymbol{E}_M]}\boldsymbol{\alpha}_M]_{I\times M}. \end{aligned} \tag{16}$$

The number of signal streams that can be spatially demultiplexed is equal to the rank of $\mathrm{rank}(\boldsymbol{W}^{\mathrm{T}}\boldsymbol{B})$. It follows from Sylvester inequality [30] that

$$\begin{aligned}&\mathrm{rank}(\boldsymbol{W}^{\mathrm{T}}\boldsymbol{B}) \geqslant \mathrm{rank}(\boldsymbol{W}) + \mathrm{rank}(\boldsymbol{B}) - I,\\&\mathrm{rank}(\boldsymbol{W}^{\mathrm{T}}\boldsymbol{B}) \leqslant \min\left\{\mathrm{rank}(\boldsymbol{W}), \mathrm{rank}(\boldsymbol{B})\right\}.\end{aligned} \tag{17}$$

In the space-isomeric array, we design $\boldsymbol{W}^{\mathrm{T}}$ such that it is a full column rank matrix, $\mathrm{rank}(\boldsymbol{W}) = I \leqslant N$. Therefore,

$$\begin{aligned}&\mathrm{rank}(\boldsymbol{W}^{\mathrm{T}}\boldsymbol{B}) \geqslant \mathrm{rank}(\boldsymbol{B}),\\&\mathrm{rank}(\boldsymbol{W}^{\mathrm{T}}\boldsymbol{B}) \leqslant \min\left\{\mathrm{rank}(\boldsymbol{W}), \mathrm{rank}(\boldsymbol{B})\right\},\end{aligned} \tag{18}$$

since $\mathrm{rank}(\boldsymbol{B}) \leqslant I = \mathrm{rank}(\boldsymbol{W})$, then

$$\mathrm{rank}(\boldsymbol{W}^{\mathrm{T}}\boldsymbol{B}) = \mathrm{rank}(\boldsymbol{B}). \tag{19}$$

When M sources are at different locations, the probability of linear correlation between the multipath channels they experience is minimal, so that $\boldsymbol{B}$ can be considered as full rank, then

$$\mathrm{rank}(\boldsymbol{B}) = \min\left\{I, M\right\}. \tag{20}$$

Since the receiver determines I, we can make $I = N$ under the condition of $\boldsymbol{W}^{\mathrm{T}}$ full rank, so that

$$\mathrm{rank}(\boldsymbol{B}) = \min\left\{N, M\right\}. \tag{21}$$

Therefore, when $M = N$, $\mathrm{rank}(\boldsymbol{W}^{\mathrm{T}}\boldsymbol{B}) = \mathrm{rank}(\boldsymbol{B}) = N$, the spatial demultiplexing of N-stream signals can be achieved.

In contrast, in the isomorphic array, $\boldsymbol{w}_1, \ldots, \boldsymbol{w}_N$ are the same, so the rank of $\boldsymbol{W}^{\mathrm{T}}\boldsymbol{B}$ is 1. In this condition, the array can hardly separate received signals even if it equips many antennas and the multipath is abundant.

3.2 Time-isomeric array

Compared with conventional arrays, space-isomeric arrays can further utilize the space resources brought by the difference between paths and realize spatial diversity and multiplexing/demultiplexing even when the antenna spacing is small. This feature triggers us to think further: if each antenna can rapidly switch patterns in a short time, then this antenna can be treated as a space-isomeric array with all antennas placed at the same position, as shown in Figure 4. Thus, the performance of the whole array can be further improved. We call such an array the time-isomeric array.

For example, assuming that the antenna n cyclically switches the patterns K times with time interval $\Delta\tau$, during which the paths of the signal are invariant, the received signal for each time can be obtained from (7), as follows:

$$y_n^{(k)} = \sum_{m=1}^{M}\sum_{l=1}^{L_m}\phi_n^{(k)}(\boldsymbol{e}_{ml})\alpha_{ml}\mathrm{e}^{\mathrm{j}2\pi f_c(k-1)\Delta\tau}x_m + z_n^{(k)}. \tag{22}$$

For antenna n, $\phi_n^{(k)}$ is the pattern of the kth switch, $y_n^{(k)}$ is the received signal at that moment, and $z_n^{(k)}$ is the noise. As a single antenna is employed, there is no array factor in (22). Using $\phi_n^{(1)}$ at time 0, the elapsed time when switching to $\phi_n^{(k)}$ is $(k-1)\Delta\tau$, and $\mathrm{e}^{\mathrm{j}2\pi f_c(k-1)\Delta\tau}$ represents the phase offset of the received signal at this time.

By substituting (4) into (22), we obtain

$$y_n^{(k)} = \sum_{m=1}^{M}x_m\sum_{l=1}^{L_m}\sum_{i=1}^{I}v_{ni}^{(k)}\mathrm{e}^{\frac{-\mathrm{j}2\pi\boldsymbol{q}_i^{\mathrm{T}}\boldsymbol{e}_{ml}}{\lambda}}\alpha_{ml} + z_n^{(k)}, \tag{23}$$

where $v_{ni}^{(k)} = w_{ni}^{(k)}\mathrm{e}^{\mathrm{j}2\pi f_c(k-1)\Delta\tau}$. By grouping the signals according to the directional diagram used in reception, a single antenna can output K signal streams, expressed in the following form:

$$\begin{bmatrix} y_n^{(1)} \\ \vdots \\ y_n^{(K)} \end{bmatrix} = \begin{bmatrix} \left(\boldsymbol{v}_n^{(1)}\right)^{\mathrm{T}}\boldsymbol{A}_{[\boldsymbol{Q}^{\mathrm{T}}\boldsymbol{E}_1]}\boldsymbol{\alpha}_1 & \cdots & \left(\boldsymbol{v}_n^{(1)}\right)^{\mathrm{T}}\boldsymbol{A}_{[\boldsymbol{Q}^{\mathrm{T}}\boldsymbol{E}_M]}\boldsymbol{\alpha}_M \\ \vdots & \ddots & \vdots \\ \left(\boldsymbol{v}_n^{(K)}\right)^{\mathrm{T}}\boldsymbol{A}_{[\boldsymbol{Q}^{\mathrm{T}}\boldsymbol{E}_1]}\boldsymbol{\alpha}_1 & \cdots & \left(\boldsymbol{v}_n^{(K)}\right)^{\mathrm{T}}\boldsymbol{A}_{[\boldsymbol{Q}^{\mathrm{T}}\boldsymbol{E}_M]}\boldsymbol{\alpha}_M \end{bmatrix} \begin{bmatrix} x_1 \\ \vdots \\ x_M \end{bmatrix} + \begin{bmatrix} z_n^{(1)} \\ \vdots \\ z_n^{(K)} \end{bmatrix}. \tag{24}$$

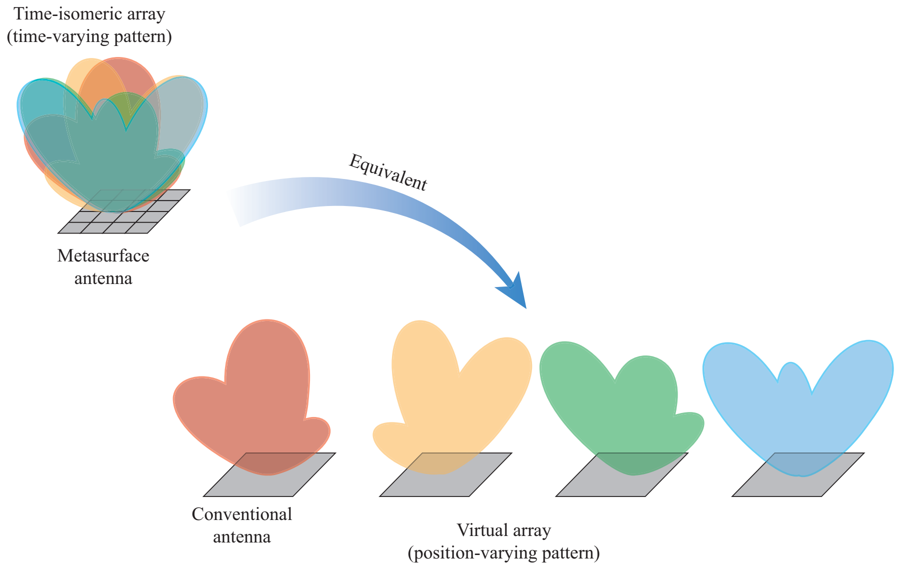

Figure 4 (Color online) In a time-isomeric array, each antenna can rapidly switch patterns in a short time so that each antenna is equivalent to a space-isomeric array with all antennas placed at the same position.

Eq. (24) can be rewritten in the following form:

$$\begin{bmatrix} y_n^{(1)} \\ \vdots \\ y_n^{(K)} \end{bmatrix} = \begin{bmatrix} \left(\boldsymbol{v}_n^{(1)}\right)^{\mathrm{T}} \\ \vdots \\ \left(\boldsymbol{v}_n^{(K)}\right)^{\mathrm{T}} \end{bmatrix} \begin{bmatrix} \boldsymbol{A}_{[\boldsymbol{Q}^{\mathrm{T}}\boldsymbol{E}_1]}\boldsymbol{\alpha}_1 & \cdots & \boldsymbol{A}_{[\boldsymbol{Q}^{\mathrm{T}}\boldsymbol{E}_M]}\boldsymbol{\alpha}_M \end{bmatrix} \begin{bmatrix} x_1 \\ \vdots \\ x_M \end{bmatrix} + \begin{bmatrix} z_n^{(1)} \\ \vdots \\ z_n^{(K)} \end{bmatrix}. \tag{25}$$

Obviously, comparing (25) with (15), we can see that they have the same form. So similar to Theorem 1, we give the theorem for the time-isomeric array as follows.

Theorem 2. For a time-isomeric array with array DOF of 1, the spatial demultiplexing of K-stream signals can be achieved by rapidly changing patterns K times within a single symbol period, i.e., the effective DOF is K.

Proof. We denote

$$\begin{aligned} \boldsymbol{V}_n &\triangleq [\boldsymbol{v}_n^{(1)}, \ldots, \boldsymbol{v}_n^{(K)}]_{I\times K}, \\ \boldsymbol{B} &\triangleq [\boldsymbol{A}_{[\boldsymbol{Q}^{\mathrm{T}}\boldsymbol{E}_1]}\boldsymbol{\alpha}_1, \ldots, \boldsymbol{A}_{[\boldsymbol{Q}^{\mathrm{T}}\boldsymbol{E}_M]}\boldsymbol{\alpha}_M]_{I\times M}, \end{aligned} \tag{26}$$

the number of signal streams that can be spatially demultiplexed is equal to $\mathrm{rank}(\boldsymbol{V}_n^{\mathrm{T}}\boldsymbol{B})$. It follows from Sylvester inequality [30] that

$$\begin{aligned} &\mathrm{rank}(\boldsymbol{V}^{\mathrm{T}}\boldsymbol{B}) \geqslant \mathrm{rank}(\boldsymbol{V}) + \mathrm{rank}(\boldsymbol{B}) - I, \\ &\mathrm{rank}(\boldsymbol{V}^{\mathrm{T}}\boldsymbol{B}) \leqslant \min\{\mathrm{rank}(\boldsymbol{V}), \mathrm{rank}(\boldsymbol{B})\}. \end{aligned} \tag{27}$$

In the time-isomeric array, using the ability of the metasurface antenna to change the pattern quickly, one can make $\boldsymbol{V}^{\mathrm{T}}$ full column rank, namely, $\mathrm{rank}(\boldsymbol{V}) = I \leqslant K$. In this case, we have

$$\mathrm{rank}(\boldsymbol{B}) \leqslant \mathrm{rank}(\boldsymbol{V}^{\mathrm{T}}\boldsymbol{B}) \leqslant \min\{\mathrm{rank}(\boldsymbol{V}), \mathrm{rank}(\boldsymbol{B})\}. \tag{28}$$

Since $\mathrm{rank}(\boldsymbol{B}) \leqslant I = \mathrm{rank}(\boldsymbol{V})$, we have

$$\mathrm{rank}(\boldsymbol{V}^{\mathrm{T}}\boldsymbol{B}) = \mathrm{rank}(\boldsymbol{B}). \tag{29}$$

As Theorem 1, it can be considered that $\boldsymbol{B}$ is full rank, so $\mathrm{rank}(\boldsymbol{B}) = \min\{I, M\}$. Let $K = I$, then

$$\mathrm{rank}(\boldsymbol{B}) = \min\{K, M\}. \tag{30}$$

Therefore, when $M = K$, $\mathrm{rank}(\boldsymbol{V}^{\mathrm{T}}\boldsymbol{B}) = \mathrm{rank}(\boldsymbol{B}) = K$, the spatial demultiplexing of K-stream signals can be achieved.

The antennas in the isomorphic array do not have the pattern switch capability, so the rank of $\boldsymbol{V}^{\mathrm{T}}\boldsymbol{B}$ is 1, and it cannot separate signals by using a single antenna.

As we can see, the time-isomeric array can be treated equivalently to a space-isomeric array in which multiple antennas are located at the same physical position, but there are also some differences. After the time-isomeric array samples the signal by rapidly changing the pattern, the sampled value is reorganized into K stream data, and the kth signal can be regarded as the result of sampling the signal using the pattern ϕ_k, with a sampling interval of $K\Delta\tau$. In order to ensure that no sampling information is lost, the sampling rate needs to satisfy Nyquist's sampling theorem, that is

$$\mathrm{Bandwidth}_x^{(k)} \leqslant \frac{1}{K\Delta\tau}, \tag{31}$$

where $\mathrm{Bandwidth}_x^{(k)}$ denotes the bandwidth of the incident signal x at moment k.

It should be noted that the virtual array formed by the metasurface antennas in this subsection is different from those in existing studies of sparse array [31, 32]. The sparse array can achieve the same performance as a conventional array with fewer antennas by changing how antennas are arranged. The sparse array enhances the DOF by changing the array structure, while the proposed method modifies the antenna structure. The metasurface antennas increase the DOF of the antenna itself by using time isomerism, which further enhances the effective DOF of the array. The two are not contradictory and can be combined. For example, to improve performance, we can use metasurface antennas to replace the classical isomorphic antennas employed in the sparse array. The application of this field can be a following study and will not be discussed in this paper.

3.3 SPATIO array

If each antenna in the space-isomeric array is independently time-isomeric, we can construct a SPATIO array whose unified model is as follows:

$$\begin{bmatrix} y_1^{(1)} \\ \vdots \\ y_1^{(K)} \\ \vdots \\ y_N^{(1)} \\ \vdots \\ y_N^{(K)} \end{bmatrix} = \begin{bmatrix} \left(\boldsymbol{v}_1^{(1)}\right)^{\mathrm{T}} \boldsymbol{A}_{[(\boldsymbol{P}_1+\boldsymbol{Q})^{\mathrm{T}}\boldsymbol{E}_1]}\boldsymbol{\alpha}_1 & \cdots & \left(\boldsymbol{v}_1^{(1)}\right)^{\mathrm{T}} \boldsymbol{A}_{[(\boldsymbol{P}_1+\boldsymbol{Q})^{\mathrm{T}}\boldsymbol{E}_M]}\boldsymbol{\alpha}_M \\ \vdots & \ddots & \vdots \\ \left(\boldsymbol{v}_1^{(K)}\right)^{\mathrm{T}} \boldsymbol{A}_{[(\boldsymbol{P}_1+\boldsymbol{Q})^{\mathrm{T}}\boldsymbol{E}_1]}\boldsymbol{\alpha}_1 & \cdots & \left(\boldsymbol{v}_1^{(K)}\right)^{\mathrm{T}} \boldsymbol{A}_{[(\boldsymbol{P}_1+\boldsymbol{Q})^{\mathrm{T}}\boldsymbol{E}_M]}\boldsymbol{\alpha}_M \\ \vdots & \ddots & \vdots \\ \left(\boldsymbol{v}_N^{(1)}\right)^{\mathrm{T}} \boldsymbol{A}_{[(\boldsymbol{P}_N+\boldsymbol{Q})^{\mathrm{T}}\boldsymbol{E}_1]}\boldsymbol{\alpha}_1 & \cdots & \left(\boldsymbol{v}_N^{(1)}\right)^{\mathrm{T}} \boldsymbol{A}_{[(\boldsymbol{P}_N+\boldsymbol{Q})^{\mathrm{T}}\boldsymbol{E}_M]}\boldsymbol{\alpha}_M \\ \vdots & \ddots & \vdots \\ \left(\boldsymbol{v}_N^{(K)}\right)^{\mathrm{T}} \boldsymbol{A}_{[(\boldsymbol{P}_N+\boldsymbol{Q})^{\mathrm{T}}\boldsymbol{E}_1]}\boldsymbol{\alpha}_1 & \cdots & \left(\boldsymbol{v}_N^{(K)}\right)^{\mathrm{T}} \boldsymbol{A}_{[(\boldsymbol{P}_N+\boldsymbol{Q})^{\mathrm{T}}\boldsymbol{E}_M]}\boldsymbol{\alpha}_M \end{bmatrix} \begin{bmatrix} x_1 \\ \vdots \\ x_M \end{bmatrix} + \begin{bmatrix} z_1^{(1)} \\ \vdots \\ z_1^{(K)} \\ \vdots \\ z_N^{(1)} \\ \vdots \\ z_N^{(K)} \end{bmatrix}, \tag{32}$$

where

$$\begin{aligned} &\boldsymbol{V}_n \triangleq [\boldsymbol{v}_n^{(1)}, \ldots, \boldsymbol{v}_n^{(K)}], \\ &\boldsymbol{B}_n \triangleq [\boldsymbol{A}_{[(\boldsymbol{P}_n+\boldsymbol{Q})^{\mathrm{T}}\boldsymbol{E}_1]}\boldsymbol{\alpha}_1, \ldots, \boldsymbol{A}_{[(\boldsymbol{P}_n+\boldsymbol{Q})^{\mathrm{T}}\boldsymbol{E}_M]}\boldsymbol{\alpha}_M], \\ &\boldsymbol{y}_n \triangleq [y_n^{(1)}, \ldots, y_n^{(K)}]^{\mathrm{T}}, \\ &\boldsymbol{x} \triangleq [x_1, \ldots, x_M]^{\mathrm{T}}, \\ &\boldsymbol{z}_n \triangleq [z_n^{(1)}, \ldots, z_n^{(K)}]^{\mathrm{T}}. \end{aligned} \tag{33}$$

Eq. (32) can be simplified in block matrix form as follows:

$$\begin{bmatrix} \boldsymbol{y}_1 \\ \vdots \\ \boldsymbol{y}_N \end{bmatrix} = \begin{bmatrix} \boldsymbol{V}_1^{\mathrm{T}} & & \\ & \ddots & \\ & & \boldsymbol{V}_N^{\mathrm{T}} \end{bmatrix} \begin{bmatrix} \boldsymbol{B}_1 \\ \vdots \\ \boldsymbol{B}_N \end{bmatrix} \boldsymbol{x} + \begin{bmatrix} \boldsymbol{z}_1 \\ \vdots \\ \boldsymbol{z}_N \end{bmatrix}. \tag{34}$$

As we can see from (34), compared to the classical MIMO system, the SPATIO array can utilize two-dimensional isomerism in the space and time domains. For the multipath channel $\boldsymbol{B}_n$, the effective DOF can be improved by modifying $\boldsymbol{V}_n$. Space isomerism increases the difference among superposed multipath channels at different antennas so that the effective DOF is the same as the array DOF at all times. The time isomerism makes each antenna equivalent to a multi-antenna array, further increasing the effective DOF. In conclusion, we can derive the following result directly from Theorems 1 and 2.

Corollary 1. The SPATIO array can obtain $N \times K$ effective DOF by the space isomerism of N antennas and the time isomerism generated by K rapid changes in the pattern of each antenna under the condition that the array DOF is N.

The SPATIO array described above is a generalized model for narrowband conditions. If the values in $\boldsymbol{v}_n^{(k)}$ are the same for any n, k, the reception model will become a classical MIMO array model, which is an isomorphic array model. Therefore, the classical MIMO array is a specific case of the SPATIO array.

The steering vectors are the responses of all antennas in the array to the arrival paths, which consist of a manifold matrix. In conventional MIMO, the manifold matrix is only determined by the geometric arrangement of the antennas. In the SPATIO array model, we can rewrite (34) as following:

$$\begin{bmatrix} \boldsymbol{y}_1 \\ \vdots \\ \boldsymbol{y}_N \end{bmatrix} = \boldsymbol{F} \begin{bmatrix} \boldsymbol{\alpha}_1 & & \\ & \ddots & \\ & & \boldsymbol{\alpha}_M \end{bmatrix} \boldsymbol{x} + \begin{bmatrix} \boldsymbol{z}_1 \\ \vdots \\ \boldsymbol{z}_N \end{bmatrix}, \tag{35}$$

where

$$\boldsymbol{F} = \begin{bmatrix} \boldsymbol{V}_1^{\mathrm{T}} & & \\ & \ddots & \\ & & \boldsymbol{V}_N^{\mathrm{T}} \end{bmatrix} \begin{bmatrix} \boldsymbol{A}_{[(\boldsymbol{P}_1+\boldsymbol{Q})^{\mathrm{T}}\boldsymbol{E}_1]} & \cdots & \boldsymbol{A}_{[(\boldsymbol{P}_1+\boldsymbol{Q})^{\mathrm{T}}\boldsymbol{E}_M]} \\ \vdots & \ddots & \vdots \\ \boldsymbol{A}_{[(\boldsymbol{P}_N+\boldsymbol{Q})^{\mathrm{T}}\boldsymbol{E}_1]} & \cdots & \boldsymbol{A}_{[(\boldsymbol{P}_N+\boldsymbol{Q})^{\mathrm{T}}\boldsymbol{E}_M]} \end{bmatrix}. \tag{36}$$

In (35), $\boldsymbol{F}$ is the manifold matrix as a function of multipath arrival directions $\boldsymbol{E}_1, \ldots, \boldsymbol{E}_M$. Obviously, a new manifold matrix can only be formed for isomorphic arrays when antenna positions $\boldsymbol{P}_1, \ldots, \boldsymbol{P}_N$ changed. However, by changing patterns, the SPATIO array can also obtain a new manifold matrix, which can be equivalent to changing the geometric arrangement of antennas. From the perspective of the array manifold, the SPATIO array can take advantage of the isomerism of the metasurface antenna to generate a new one-dimensional DOF and form a flexible array structure. Thus the SPATIO array can optimize the array design from a higher dimension. Next, we will propose a SPATIO array reception scheme for multi-stream signal reception.

3.4 Multi-stream signal reception based on INM

In MIMO systems, two problems need to be solved for multi-stream signal reception: the separation of multi-stream signals by utilizing the difference of spatial domain and the optimal energy reception for each stream. In an isomorphic array system, the antenna passively collects the incoming wave, while the backend superposes signal energy and separates different signal streams. The mismatch between pattern and multipath will lead to the loss of effective DOF and energy, resulting in the loss of received information. From the information theory perspective, backend signal processing cannot recover this lost information.

However, the SPATIO array, on the one hand, can match the multipath by adjusting the pattern of each antenna at a distinct position. On the other hand, it can utilize time isomerism to realize the array design for different signals at different moments.

Assume that a SPATIO array with N antennas is capable of rapidly changing the pattern K times within a single symbol period, receiving the transmitted signals from M streams, $N \geqslant M = K$, and only signals from stream k are received at the moment k, that is

$$\sum_{n=1}^{N} y_n^{(k)} = \left[\left(\boldsymbol{v}_1^{(k)}\right)^{\mathrm{T}} \cdots \left(\boldsymbol{v}_N^{(k)}\right)^{\mathrm{T}} \right] \begin{bmatrix} \boldsymbol{B}_1 \\ \vdots \\ \boldsymbol{B}_N \end{bmatrix} \begin{bmatrix} x_1 \\ \vdots \\ x_M \end{bmatrix} + \sum_{n=1}^{N} z_n^{(k)} = C_k x_k + \sum_{n=1}^{N} z_n^{(k)}, \tag{37}$$

where $C_k \in \mathbb{R}^+$ is the array gain on the signal x_k at the moment k array. We want C_k to be as large as possible. For a metasurface antenna, each element is capable of adjusting the phase of the incident signal and performing attenuation, so $|v_{ni}^{(k)}| \leqslant 1$. The design of the SPATIO array can be summarized as the following optimization problem:

$$\begin{aligned} \max_{\boldsymbol{v}_1^{(k)},\ldots,\boldsymbol{v}_N^{(k)}} \quad & C_k \\ \text{s.t.} \quad & \begin{bmatrix} \boldsymbol{B}_1^{\mathrm{T}} & \cdots & \boldsymbol{B}_N^{\mathrm{T}} \end{bmatrix} \begin{bmatrix} \boldsymbol{v}_1^{(k)} \\ \vdots \\ \boldsymbol{v}_N^{(k)} \end{bmatrix} = \begin{bmatrix} 0 \\ \vdots \\ C_k \\ \vdots \\ 0 \end{bmatrix}, \\ & \left| v_{ni}^{(k)} \right| \leqslant 1, 1 \leqslant n \leqslant N, 1 \leqslant i \leqslant I. \end{aligned} \tag{38}$$

The second constraint is equivalent to $\max_{n,i} |v_{ni}^{(k)}| \leqslant 1$. We denote that $\bar{v}_{ni}^{(k)} = v_{ni}^{(k)}/C_k$, then the problem can be rewritten as

$$\begin{aligned} \max_{\bar{\boldsymbol{v}}_1^{(k)},\ldots,\bar{\boldsymbol{v}}_N^{(k)}} \quad & C_k = \frac{1}{\max_{n,i} |\bar{v}_{ni}^{(k)}|} \\ \text{s.t.} \quad & \begin{bmatrix} \boldsymbol{B}_1^{\mathrm{T}} & \cdots & \boldsymbol{B}_N^{\mathrm{T}} \end{bmatrix} \begin{bmatrix} \bar{\boldsymbol{v}}_1^{(k)} \\ \vdots \\ \bar{\boldsymbol{v}}_N^{(k)} \end{bmatrix} = \begin{bmatrix} 0 \\ \vdots \\ 1 \\ \vdots \\ 0 \end{bmatrix}. \end{aligned} \tag{39}$$

We have already proposed the multipath channel estimation scheme in our previous study [33] and assume that accurate multipath channel state information $\boldsymbol{B}_n$ can be obtained here. Because

$$\max_{\bar{\boldsymbol{v}}_1^{(k)},\ldots,\bar{\boldsymbol{v}}_N^{(k)}} \frac{1}{\max_{n,i} |\bar{v}_{ni}^{(k)}|} = \min_{\bar{\boldsymbol{v}}_1^{(k)},\ldots,\bar{\boldsymbol{v}}_N^{(k)}} \left\| \left[\left(\bar{\boldsymbol{v}}_1^{(k)} \right)^{\mathrm{T}}, \ldots, \left(\bar{\boldsymbol{v}}_N^{(k)} \right)^{\mathrm{T}} \right] \right\|_\infty, \tag{40}$$

where $\|\cdot\|_\infty$ denotes the infinity norm, we can obtain C_k in two steps as follows.

First, we solve the following INM [34] problem:

$$\begin{aligned} \min_{\bar{\boldsymbol{v}}_1^{(k)},\ldots,\bar{\boldsymbol{v}}_N^{(k)}} \quad & \left\| \left[\left(\bar{\boldsymbol{v}}_1^{(k)} \right)^{\mathrm{T}}, \ldots, \left(\bar{\boldsymbol{v}}_N^{(k)} \right)^{\mathrm{T}} \right] \right\|_\infty \\ \text{s.t.} \quad & \begin{bmatrix} \boldsymbol{B}_1^{\mathrm{T}} & \cdots & \boldsymbol{B}_N^{\mathrm{T}} \end{bmatrix} \begin{bmatrix} \bar{\boldsymbol{v}}_1^{(k)} \\ \vdots \\ \bar{\boldsymbol{v}}_N^{(k)} \end{bmatrix} = \begin{bmatrix} 0 \\ \vdots \\ 1 \\ \vdots \\ 0 \end{bmatrix}. \end{aligned} \tag{41}$$

Then calculate every $\boldsymbol{v}_n^{(k)}$ as follows:

$$\boldsymbol{v}_n^{(k)} = C_k \bar{\boldsymbol{v}}_n^{(k)} = \frac{\bar{\boldsymbol{v}}_n^{(k)}}{\max_{n,i} |\bar{v}_{ni}^{(k)}|}. \tag{42}$$

After solving (41) and (42), we obtain the array design parameters of k, just repeating the above process to complete the SPATIO array design.

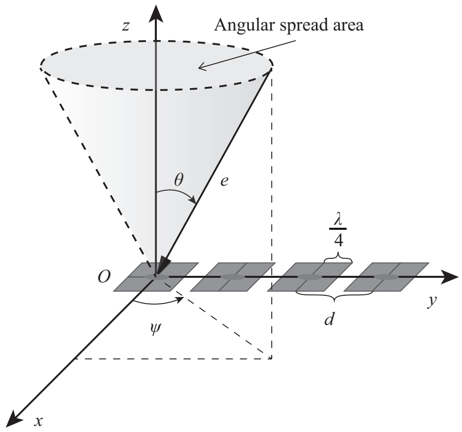

Figure 5 Structure of metasurface antennas and their arrangement in SPATIO array for the simulation. In our simulation, four metasurface antennas are uniformly arranged in the positive direction of the y-axis from the coordinate origin. Each antenna has four metamaterial elements, centered at the antenna location, which is arranged in a 2×2 rectangle.

4 Simulation and numerical results

In this section, we verify the feasibility of the proposed SPATIO array in this paper and demonstrate the performance of the proposed optimization algorithm by computer simulations. If not explicitly explained, the parameters used in the simulations will be configured as follows.

As shown in Figure 5, the system operates in the 2.4 GHz band, and the receiver is equipped with $N = 4$ antennas, all of which are metasurface antennas with adjustable element states. The antenna spacing is $\frac{\lambda}{2}$, uniformly arranged in the positive direction of the y-axis from the coordinate origin. The number of metamaterial elements I on each antenna is 4, centered at the antenna location, which is arranged in a 2×2 rectangle, and the adjacent elements are with spacing $\frac{\lambda}{4}$. Each element is independent and can be either attenuated or phase-shifted to the arriving signal, with an attenuation range of $[0, 1]$ and an adjustable phase range of $[0, 2\pi)$. Each antenna can rapidly change $K = 4$ times within a single receive symbol period.

The transmitter sends $M = 4$ streams, which are transmitted to the receiver through a multipath channel containing 1000 QPSK (quadrature phase shift keying) symbols per stream with a signal-to-noise ratio (SNR) of 10 dB. The paths are independent of each other and kept constant during one cycle. The number of paths is randomly and uniformly selected among $[2, 6]$ for each stream, referring to the spatial channel model (SCM) and spatial channel model extension (SCME) channel models [35]. The multipath direction vector points to the receiving array, and the incident angles follow a uniform distribution with the elevation θ angular spread range of $[0, 45]$ degrees and the azimuth ψ angular spread range of $[0, 360]$ degrees. The path complex gains are all independent and follow the Gaussian distribution. For stream m, the path complex gain follows $\mathcal{CN}(0, \frac{1}{L_m})$, where L_m is the number of paths in stream m, and the sum energy of paths in each stream can be the same in this way.

According to the above simulation conditions, we compare the performance of the three types of array configurations by averaging the results of 10000 Monte Carlo simulations at each point.

- INM based configuration. According to the proposed method in Subsection 3.4, we calculate the metasurface antenna elements states for the current multipath channel to achieve optimal reception while ensuring multi-stream signal separation.
- Random weight (RandW) based configuration. All antenna elements are only phase-shifted to the incident signal without causing amplitude attenuation, and the phase-shifted value of each element is chosen randomly among $(0, 2\pi]$. When the complete multipath channel information is unavailable, the SPATIO array can also reduce the correlation of channels between antennas by randomly configuring the element weights to improve the multi-stream separation performance under space-constrained conditions. This is another way of using array isomerism, so we compared the proposed method with it.
- Isomorphic based configuration. The array is a conventional isomorphic MIMO array when all antenna elements are configured with the same state. Without loss of generality, in this configuration, let the complex gain of all elements be 1, that is, $|v_{ni}^{(k)}| = 1$.

4.1 Simulation performance indicators: condition number and bit error rate

We use the condition number (CN) of the composite channel matrix and the bit error rate (BER) of the received signal to measure the system performance.

As shown in (32), the channel matrix of the SPATIO array consists of two parts, the natural multipath channel $\boldsymbol{B}_n$ and the antenna configuration parameter $\boldsymbol{V}_n$. So we can use the CN of the composite channel, including the above two, to describe the multi-stream signal separation capability.

The CN $\kappa(\boldsymbol{H})$ is defined as the ratio of the maximum singular value to the minimum singular value of the channel matrix $\boldsymbol{H}$, as follows:

$$\kappa(\boldsymbol{H}) = \frac{\sigma_{\max}}{\sigma_{\min}},$$
$$\boldsymbol{H} \triangleq \begin{bmatrix} \boldsymbol{V}_1^{\mathrm{T}} & & \\ & \ddots & \\ & & \boldsymbol{V}_N^{\mathrm{T}} \end{bmatrix} \begin{bmatrix} \boldsymbol{B}_1 \\ \vdots \\ \boldsymbol{B}_N \end{bmatrix}. \tag{43}$$

The MIMO channel can be divided into several independent subchannels through singular value decomposition. Each subchannel transmits one stream, and the larger the singular value, the better the channel quality. A small CN means that the subchannels are of similar quality and can be separated. Conversely, a large CN means there are poor quality subchannels, and the signals transmitted in these subchannels are challenging to recover.

The CN directly reflects the maximum multi-stream signal separation capability the current channel can achieve. In contrast, the BER demonstrates the effect of noise and inter-stream interference after signal separation. The SPATIO array can modulate $\boldsymbol{V}_n$ to change $\boldsymbol{H}$, thus lowering the CN and BER.

4.2 Effect of SNR

Figure 6(a) shows the variation of the received BER with the SNR for three different configurations using the zero forcing (ZF) and minimum mean squared error (MMSE) signal detection algorithms, respectively. The BER decreases with increasing SNR in these conditions, and MMSE has better noise immunity than the ZF. Compared to the isomorphic configuration, the INM and RandW configuration improves the rank by changing the antenna pattern, thus reducing the interference between streams. The INM can achieve a higher energy gain than the isomorphic configuration. As a result, the SPATIO array has a lower BER when the SNR is higher than 10 dB.

At low SNR below 5 dB, classical isomorphic MIMO systems have slightly lowered received BER than SPATIO arrays. The reason is that with the INM configuration, the array receives only one signal each time the antenna pattern switches. With limited antenna DOF, some elements attenuate the incident signal to ensure that the undesired signal is eventually filtered, resulting in reduced signal energy in the final RF channel. However, in the simulation, all the elements of the isomorphic configuration have a complex gain of 1, so the maximum gain direction of the antenna is the normal direction of the array, which is the same as the center direction of the incident multipath angle scattering. So it can get more signal energy, and the BER is relatively low.

Figure 6(b) shows the performance of the array when equipped with two antennas. The array uses two antennas in the simulation to receive four stream signals. For classical MIMO systems, multiple streams of stream signals are mixed due to the insufficient number of antennas. At the same time, SPATIO arrays can more effectively exploit the differences between paths and receive four streams even with only two antennas.

4.3 Effects of antenna interval

Figure 7(a) shows the variation of the CN with the antenna interval d. The multipath superposition difference at each antenna increases with the growth of d. Thus, the array can achieve better multi-stream reception performance. For all configuration conditions, the CN drops fast with increasing d when less than λ, then decreases at a slower rate and almost stops after it exceeds 1.5λ. The CN of INM configuration can be reduced by 6 to 10 dB compared with the isomorphic array when the antennas are close, less than λ. The CN can also be reduced by about 5 dB when d exceeds 1.5λ, so the CN is less than 10 dB, which is considered to have good multi-stream separation performance in engineering. In

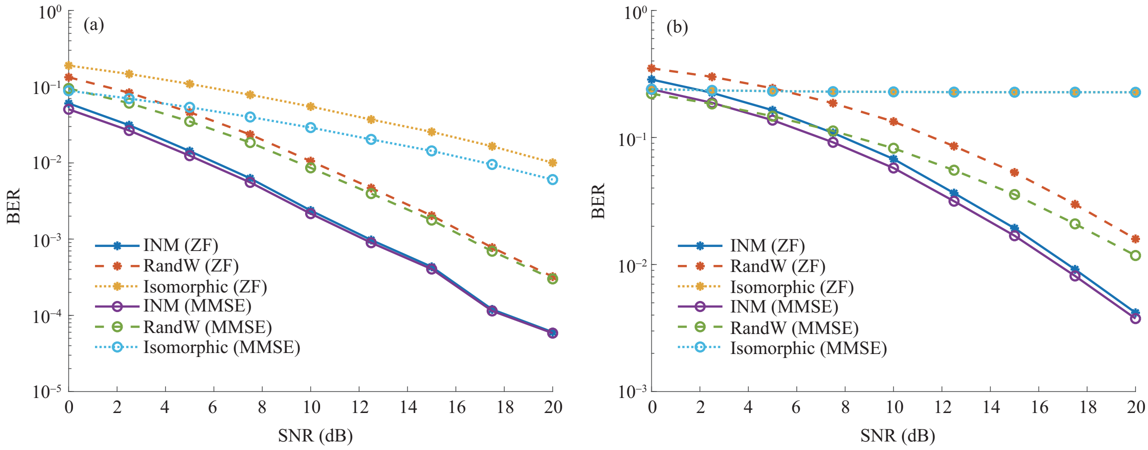

Figure 6 (Color online) Variation of the received BER with the SNR for three different configurations using the ZF and MMSE signal detection algorithms. The BER decreases with increasing SNR in these conditions, and MMSE has better noise immunity than the ZF. (a) BER varying of the array when equipped with four antennas; (b) BER varying of the array when equipped with two antennas.

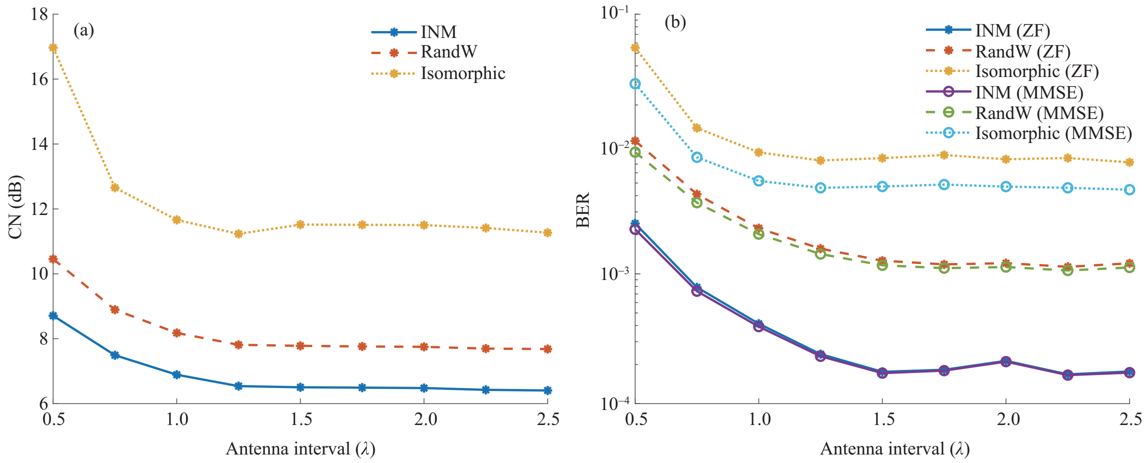

Figure 7 (Color online) Variation of CN and BER with the antenna interval. The multipath superposition difference at each antenna increases with the growth of the antenna interval, resulting in better multi-stream reception performance. For the SPATIO array, the CN can be reduced by about 5 dB when the antenna interval exceeds 1.5λ, and then the BER is less than 10^{-3}. (a) CN of composite channel matrix varying with the antenna interval; (b) BER of received signals varying with the antenna interval.

addition, even if accurate multipath channel information is unavailable, RandW configuration can still reduce the CN by 3 to 4 dB compared to an isomorphic array.

Figure 7(b) shows the BER varying with the antenna interval. The CN decreases and achieves better signal separation with increasing d. Thus the BER is consequently reduced. Compared with the isomorphic configuration, the BER can be reduced by one order of magnitude with the INM configuration when the CN decreases and achieves better signal separation with the increasing of d is less than λ and by almost two orders of magnitude when d exceeds 1.5λ. This is owing to the poor performance of the ZF and MMSE algorithms at high CN, while the SPATIO array with low CN can further exploit the performance of the algorithms.

4.4 Effects of multipath angular spread

The enlarged diversity of multipath incidence angles increases the phase difference when arriving at each antenna, thus reducing the correlation of the channel consisting of multipath superposition and improving the multi-stream reception performance. The multipath angular spread represents the size of the random distribution range of multipath incidence angles, as shown in Figures 8(a) and (b), demonstrating the effect on the CN of the composite channel as θ is varied from 5 to 60 degrees. As the multipath angular

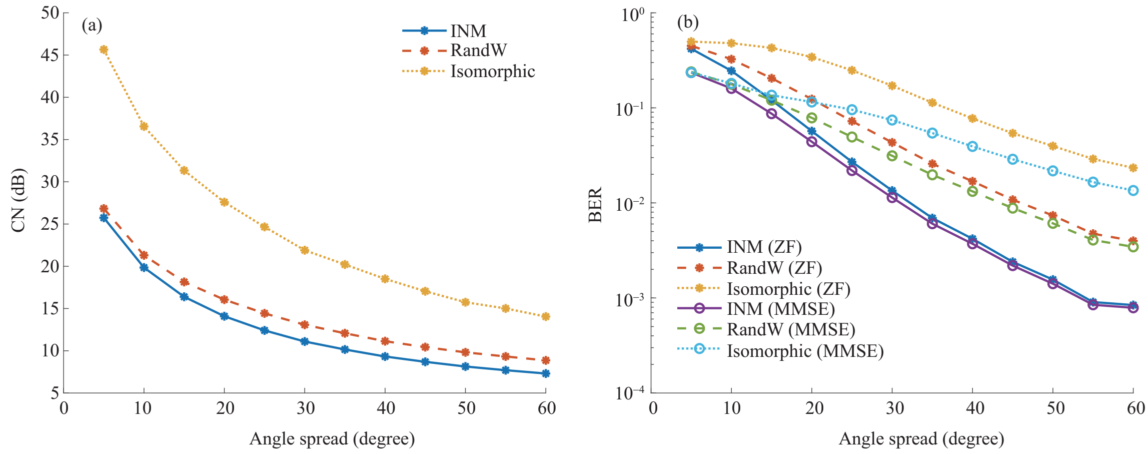

Figure 8 (Color online) Variation of CN and BER with the multipath angular spread. At high angular spreads wider than 50 degrees, the SPATIO arrays improve system performance by achieving CNs below 10 dB and reducing the BER by an order of magnitude. (a) CN of composite channel matrix varying with the multipath angular spread; (b) BER of received signals varying with the multipath angular spread.

spread increases, the CN drops rapidly so that the received BER decreases. When the angular spread is small, the paths of different streams tend to overlap. It is hard to tell the channel differences of each stream with a conventional isomorphic MIMO array. It can be seen that the CN of the isomorphic array exceeds 30 dB when the angular spread is below 15 degrees, and the energy in different sub-channels varies greatly. In the SPATIO array, the paths are superposed in various ways by varying the pattern. The spatial differences between paths are further exploited to reduce the CN by 10 to 15 dB. At high angular spreads wider than 50 degrees, the multipath superposition on each antenna is sufficiently different. The CN can be reduced to about 15 dB even for the isomorphic array. While SPATIO array with INM configurations further improves system performance by achieving CNs below 10 dB and reducing the BER by an order of magnitude.

4.5 Effects of the number of paths

Another parameter that affects multi-stream reception performance is the number of paths. Typically, increasing the number of paths can reduce the correlation between channels. To demonstrate the effect of the number of paths more precisely, in Figures 9(a) and (b), instead of the random selection of the number of paths for each stream, we make all streams have the same number of paths. It is observed that the CN decreases gradually with the increase of the number of paths when the angle scattering is 45 degrees. While increasing the number of paths from 2 to 6, the CN of the isomorphic array decreases by 5 dB, but the BER does not decrease significantly. In contrast, for the SPATIO array with INM configuration, the antennas are always matched to the current channel to maximize energy harvesting with guaranteed multi-stream signal separation, so the CN is always kept below 10 dB. The BER is reduced by one order of magnitude when the CN reduces by 2 dB.

5 Demonstration of single space-fed metasurface antenna multi-stream signals separation

In this section, we build an experimental verification platform for multi-stream signals reception using a single space-fed metasurface antenna to more intuitively demonstrate the effect of enhancing the effective DOF. As shown in Figure 10, the experimental verification platform consists of a space-fed metasurface antenna, a receiver, and a transmitter.

The space-fed metasurface antenna consists of a reconfigurable intelligent surface (RIS) [36] with a horn antenna. The RIS can adjust the incident signals' amplitude, phase, and other parameters, and then reflect them into the receiving antenna. Figure 11 shows the RIS used in this platform, which consists of 8 columns and 16 rows of metamaterial elements. The metamaterial elements in each column use the same controlling signal, while those in different columns are independent. The RIS operates in 3.15 GHz, and the size of each element is 25 mm $\times$ 27 mm, which is about $\frac{1}{4}$ of the wavelength [37]. The

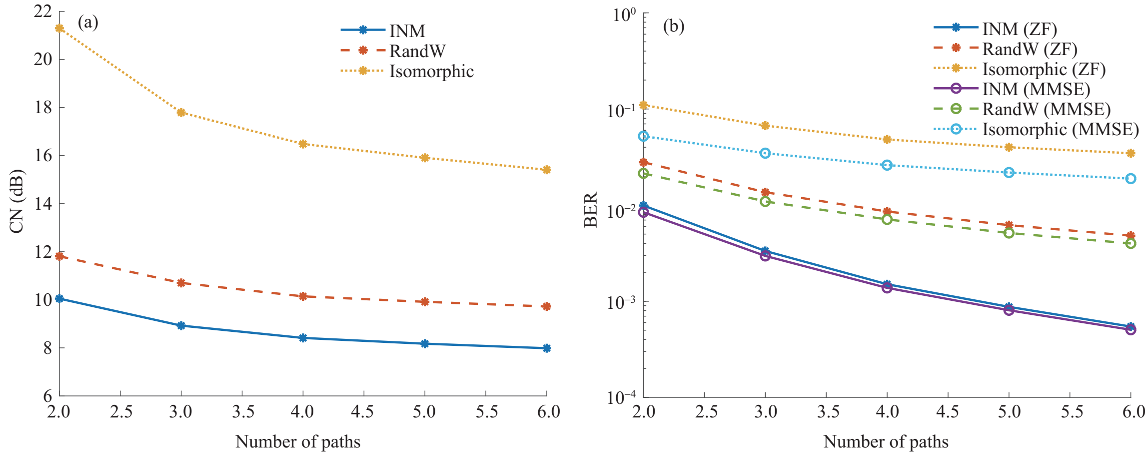

Figure 9 (Color online) Variation of CN and BER with the number of paths. For the SPATIO array, the CN is always kept below 10 dB, and the BER is reduced by one order of magnitude when the CN reduces by 2 dB. (a) CN of composite channel matrix varying with the number of paths; (b) BER of received signals varying with the number of paths.

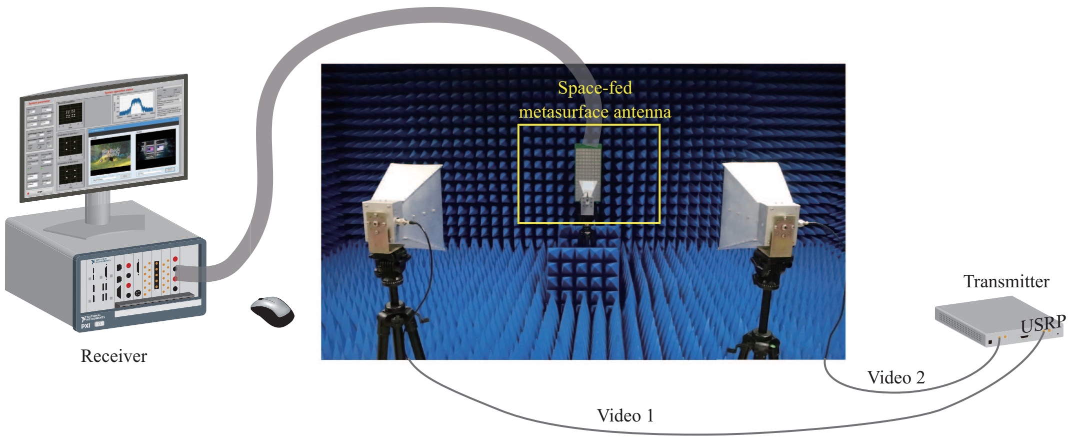

Figure 10 (Color online) Experimental verification platform for multi-stream signals reception using a single space-fed metasurface antenna.

RIS uses varactors to reconfigure the parameters, and the reflected signal phase can be adjusted in the range of $[0, 2\pi]$ by changing the input voltage. The receiving horn antenna is facing the RIS and placed on the normal. Then the received signals enter the horn antenna after being modulated by the RIS.

In recent studies, the space-fed metasurface antennas are equipped for signal modulation and transmission at the transmitter [38, 39]. The system shown in this section is the other way around, where the space-fed metasurface antennas are equipped at the receiver. The patterns of the space-fed metasurface antenna also satisfy (4), and we will give the related analysis in Appendix A.

Both the receiver and transmitter are software define radio (SDR) platforms. The receiver is built with the NI control platform, which integrates: a central controller (PXIe-8880) as the host, a field programmable gate array (FPGA) module (PXIe-7976) to control the super-surface antenna parameters, a vector signal receiver (PXIe-5841) to receive the RIS modulated signals then complete the RF signal sampling and down-conversion. The transmitter is built with NI-USRP 2953R and a host computer to generate the transmit signals and complete the modulation and up-conversion.

The structure of the transmit signal frame is shown in Figure 12. Each frame contains one synchronization frame (256 symbols), one pilot frame (256 symbols), and four service frames (4×3072 symbols). The synchronization frame is a PN sequence, while the pilot frames for different users are mutually orthogonal Walsh sequences, both modulated with BPSK (binary phase shift keying). The data are multimedia video streams with QPSK modulation and packetized according to the user datagram protocol (UDP) protocol. The transmission symbol rate is 256000 symbols per second, and the frame period is 50 ms.

In this experiment, two horn antennas send mutually independent video signals from different direc-

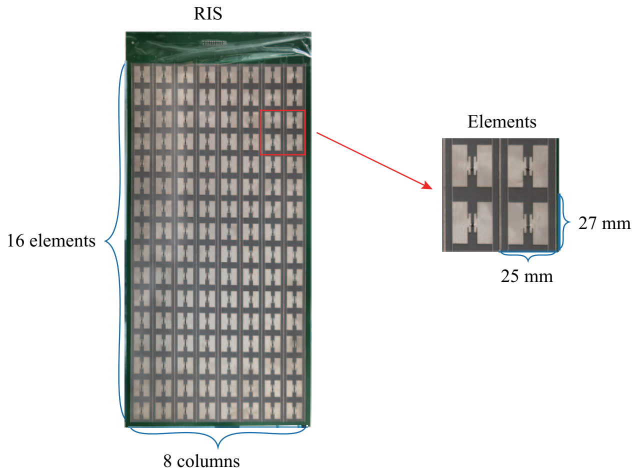

Figure 11 (Color online) Size of RIS and metasurface elements.

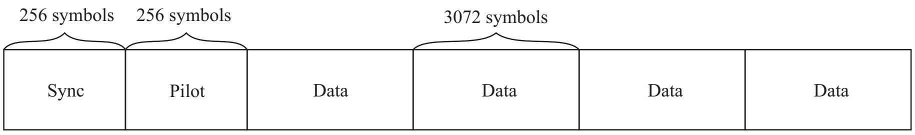

Figure 12 Frame structure of the transmit signal.

tions. The metasurface antenna receives signals by time isomerism and uses an eight-order Hadamard matrix as the code to control the pattern switching: the elements in each row of the matrix represent the phase change of the incident signals affected by the columns of metamaterial elements, where "1" means not change the phase while "-1" means invert it. Eight rows correspond to eight patterns. Since there is only one metasurface antenna, these codes are $\boldsymbol{v}_1^{(1)}, \ldots, \boldsymbol{v}_1^{(8)}$ in (24). The FPGA module controls the metasurface antenna to receive the signals by cyclically switching eight codes. According to (24), the receiver divides the signal into eight channels based on the code used at the reception. Then we use the local pilot sequence to estimate the channels, equalize the received signals, and finally separate two video signals. The video transmission bit rate is approximately 230 kbps.

The signal reception interface of the receiver is shown in Figure 13, which shows the received constellation diagrams before and after the signal separation and real-time playback of the received videos. Among them, Figure 13(a) shows the received signal constellation of the metasurface antenna with an all-1 code, which is the same as the isomorphic antenna reception. Since only one isomorphic antenna can not separate signals, the constellations of the two streams are superimposed on each other. Figure 13(b) shows the constellation after signal separation using the proposed method. The separated signals are demodulated by the receiver and restored to video, which is displayed in the video playback window Figure 13(c). The experiments show that the receiver can separate two signals using only one metasurface antenna. Compared with conventional antennas, even if they have the same reception performance, it is difficult to achieve the same signal separation function as the metasurface antenna due to the lack of DOF of the antenna itself.

6 Conclusion

This paper studied the SPATIO array model and design method based on the metasurface antenna. Under the wireless multipath channel conditions, the array utilized the flexible pattern control capability of the metasurface antenna to make each antenna in the array change its patterns independently at different moments and enhance the variability of multipath channel superposition. So the effective DOF of the array can be improved by increasing the difference of multipath channel superposition. Then we gave an antenna design scheme based on the INM. This scheme enhanced the multi-stream signal separation capability of the array while ensuring that the desired multipath energy is collected and filtering the non-desired signal, further improving the reception performance of each stream. Simulation results

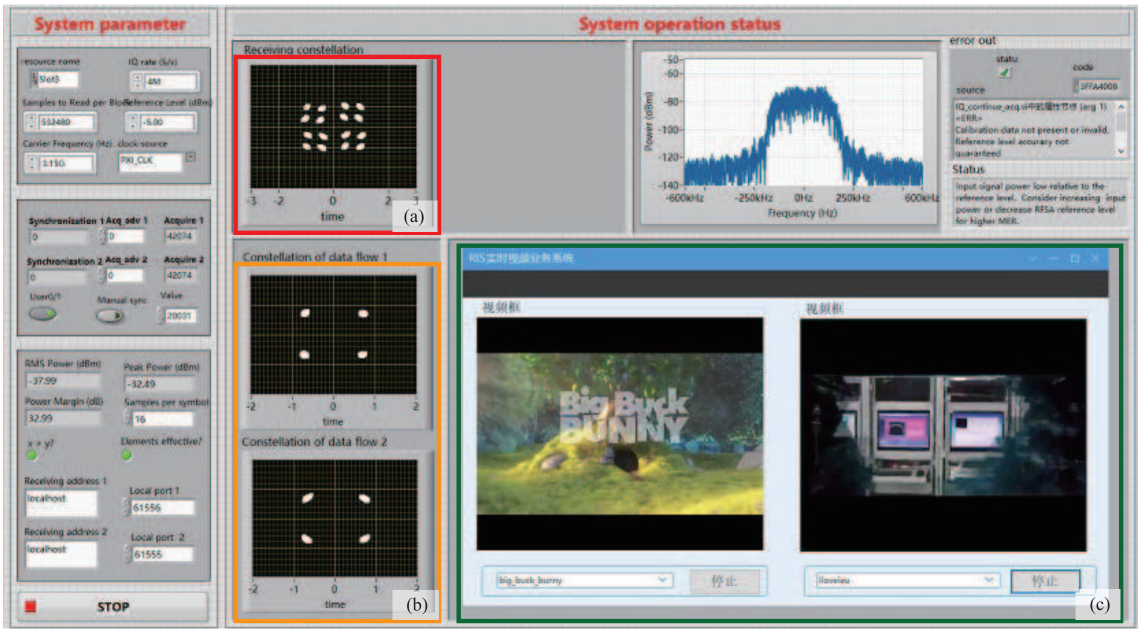

Figure 13 (Color online) Signal reception effects are shown as follows: (a) received signal constellation of the metasurface antenna with an all-1 code; (b) constellation of the separated video signals after channel equalization; (c) real-time playback window of the video signals.

demonstrated that the SPATIO array can adequately utilize multipath and improved spatial demultiplexing performance. It can reduce the BER by one order of magnitude compared to the conventional MIMO array. By building an experimental verification platform, we verified that the metamaterial antenna had multi-stream signal separation capability.

Acknowledgements This work was supported by Program of Song Shan Laboratory (included in the Management of the Major Science and Technology Program of Henan Province) (Grant Nos. 221100211300-01, 221100211300-03) and National Natural Science Foundation of China (Grant Nos. U22A2001, 62201139, 62171364).

References

1 Gupta A, Jha R K. A survey of 5G network: architecture and emerging technologies. IEEE Access, 2015, 3: 1206–1232
2 Gesbert D, Hanly S, Huang H, et al. Multi-cell MIMO cooperative networks: a new look at interference. IEEE J Sel Areas Commun, 2010, 28: 1380–1408
3 Hasan W B, Harris P, Doufexi A, et al. Impact of user number on massive MIMO with a practical number of antennas. In: Proceedings of the 87th Vehicular Technology Conference (VTC Spring), Porto, 2018. 1–5
4 Harris P, Malkowsky S, Vieira J, et al. Performance characterization of a real-time massive MIMO system with LOS mobile channels. IEEE J Sel Areas Commun, 2017, 35: 1244–1253
5 Harris P, Hasan W B, Malkowsky S, et al. Serving 22 users in real-time with a 128-antenna massive MIMO testbed. In: Proceedings of the IEEE International Workshop on Signal Processing Systems (SiPS), Dallas, 2016. 266–272
6 Shiu D S, Foschini G J, Gans M J, et al. Fading correlation and its effect on the capacity of multielement antenna systems. IEEE Trans Commun, 2000, 48: 502–513
7 Lee W C Y. Effects on correlation between two mobile radio base-station antennas. IEEE Trans Veh Technol, 1973, 22: 130–140
8 Chiao J-C, Fu Y, Chio I M, et al. MEMS reconfigurable vee antenna. In: Proceedings of the IEEE MTT-S International Microwave Symposium Digest, 1999. 1515–1518
9 Grau A, Romeu J, Ming-Jer Lee J, et al. A dual-linearly-polarized MEMS-reconfigurable antenna for narrowband MIMO communication systems. IEEE Trans Antenna Propagat, 2010, 58: 4–17
10 Nikolaou S, Kingsley N D, Ponchak G E, et al. UWB elliptical monopoles with a reconfigurable band notch using MEMS switches actuated without bias lines. IEEE Trans Antenna Propagat, 2009, 57: 2242–2251
11 Zhang J, Zhang S, Ying Z, et al. Radiation-pattern reconfigurable phased array with p-i-n diodes controlled for 5G mobile terminals. IEEE Trans Microw Theor Techn, 2020, 68: 1103–1117
12 Nikolaou S, Bairavasubramanian R, Lugo C, et al. Pattern and frequency reconfigurable annular slot antenna using PIN diodes. IEEE Trans Antenna Propagat, 2006, 54: 439–448
13 Tawk Y, Costantine J, Christodoulou C G. A varactor-based reconfigurable filtenna. Antenna Wirel Propag Lett, 2012, 11: 716–719
14 White C R, Rebeiz G M. Single- and dual-polarized tunable slot-ring antennas. IEEE Trans Antenna Propagat, 2009, 57: 19–26
15 Christodoulou C G, Tawk Y, Lane S A, et al. Reconfigurable antennas for wireless and space applications. Proc IEEE, 2012, 100: 2250–2261
16 Parchin N O, Basherlou H J, Al-Yasir Y I A, et al. Reconfigurable antennas: switching techniques-a survey. Electronics, 2020, 9: 336

17 Parchin N O, Basherlou H J, Al-Yasir Y, et al. Recent developments of reconfigurable antennas for current and future wireless communication systems. Electronics, 2019, 8: 128
18 Jin G, Li M, Liu D, et al. A simple planar pattern-reconfigurable antenna based on arc dipoles. Antenna Wirel Propag Lett, 2018, 17: 1664–1668
19 Almasi M A, Mehrpouyan H, Matolak D, et al. Reconfigurable antenna multiple access for 5G mmWave systems. In: Proceedings of the IEEE International Conference on Communications Workshops (ICC Workshops), Kansas, 2018. 1–6
20 Kiesel G, Strates E, Phillips C. Beam forming with a reconfigurable antenna array. In: Proceedings of the IEEE International Symposium on Phased Array Systems and Technology (PAST), Waltham, 2016. 1–3
21 Hunt J, Driscoll T, Mrozack A, et al. Metamaterial apertures for computational imaging. Science, 2013, 339: 310–313
22 Yoo I, Imani M F, Sleasman T, et al. Efficient complementary metamaterial element for waveguide-fed metasurface antennas. Opt Express, 2016, 24: 28686–28692
23 Yoo I, Imani M F, Sleasman T, et al. Enhancing capacity of spatial multiplexing systems using reconfigurable cavity-backed metasurface antennas in clustered MIMO channels. IEEE Trans Commun, 2019, 67: 1070–1084
24 Kong G S, Ma H F, Cai B G, et al. Continuous leaky-wave scanning using periodically modulated spoof plasmonic waveguide. Sci Rep, 2016, 6: 29600
25 Wang M, Ma H F, Tang W X, et al. Leaky-wave radiations with arbitrarily customizable polarizations based on spoof surface plasmon polaritons. Phys Rev Appl, 2019, 12: 014036
26 Wang M, Ma H F, Zhang H C, et al. Frequency-fixed beam-scanning leaky-wave antenna using electronically controllable corrugated microstrip line. IEEE Trans Antenna Propagat, 2018, 66: 4449–4457
27 Shuang Y, Zhao H T, Wei M L, et al. One-bit quantization is good for programmable coding metasurfaces. Sci China Inf Sci, 2022, 65: 172301
28 Liu X B, Xue W, Chen X M, et al. On the uniqueness of virtual substrate for metasurface in a dielectric half-space. Sci China Inf Sci, 2022, 65: 112302
29 Jin L, Lou Y, Xu X, et al. Separating multi-stream signals based on space-time isomerism. In: Proceedings of the International Conference on Wireless Communications and Signal Processing (WCSP), Nanjing, 2020. 418–423
30 Horn R A, Johnson C R. Matrix Analysis. 2nd ed. Cambridge: Cambridge University Press, 2012
31 Liu C, Vaidyanathan P P. Super nested arrays: sparse arrays with less mutual coupling than nested arrays. In: Proceedings of the IEEE International Conference on Acoustics, Speech and Signal Processing (ICASSP), Shanghai, 2016. 2976–2980
32 Shi W, Li Y, de Lamare R C. Novel sparse array design based on the maximum inter-element spacing criterion. IEEE Signal Process Lett, 2022, 29: 1754–1758
33 Lou Y, Jin L, Sun X, et al. Multi-path separation and parameter estimation by single DMA in fading channel. IET Commun, 2022, 16: 1475–1485
34 Liu T, Hoang M, Yang Y, et al. A parallel optimization approach on the infinity norm minimization problem. In: Proceedings of the 27th European Signal Processing Conference (EUSIPCO), 2019. 1–5
35 Narandzic M, Schneider C, Thoma R, et al. Comparison of SCM, SCME, and WINNER channel models. In: Proceedings of the 65th Vehicular Technology Conference, Dublin, 2007. 413–417
36 Cui T J, Qi M Q, Wan X, et al. Coding metamaterials, digital metamaterials and programmable metamaterials. Light Sci Appl, 2014, 3: e218
37 Liang J C, Cheng Q, Gao Y, et al. An angle-insensitive 3-bit reconfigurable intelligent surface. IEEE Trans Antenna Propagat, 2022, 70: 8798–8808
38 Dai J Y, Tang W, Chen M Z, et al. Wireless communication based on information metasurfaces. IEEE Trans Microw Theor Techn, 2021, 69: 1493–1510
39 Zhang L, Chen M Z, Tang W, et al. A wireless communication scheme based on space- and frequency-division multiplexing using digital metasurfaces. Nat Electron, 2021, 4: 218–227

Appendix A Signal reception models of different metasurface antennas

Metasurface antennas have various forms for application scenarios that need enough DOF, such as spatial multiplexing/demultiplexing or DoA estimation. There have been mainly two types of metasurface antennas in recent research. One is the space-fed metasurface antenna that combines RIS with the conventional antenna [36–39].By adding RIS, we can improve the system performance by providing the antenna with space-time isomerism without significantly modifying the existing receiver hardware structure. And another is the dynamic metasurface antenna (DMA) which directly connects to the transceiver by replacing the conventional antenna[1)2)3)]. This metasurface antenna is isomeric and can enhance the effective DOF. We will analyze their reception models and show that both antennas can be described by the space-time isomeric array model.

Appendix A.1 Space-fed metasurface antenna

For the space-fed metasurface antenna, the signals are reflected into the RF channel through RIS so that the channel can be divided into three parts: source to RIS, RIS weighting of the signal, and RIS to RF channel. The channel from source to RIS can be expressed as

$$\boldsymbol{h}_{\text{in}} = \boldsymbol{A}\boldsymbol{\alpha}, \tag{A1}$$

where $\boldsymbol{A}$ and $\boldsymbol{\alpha}$ denote the manifold matrix of the RIS and complex gain of the paths, respectively. We note that the RIS is weighted by $v_1^{(k)}, \ldots, v_I^{(k)}$ for each element at the sampling moment k, and the channel from the elements to the RF channel is

1) Shlezinger N, Dicker O, Eldar Y C, et al. Dynamic metasurface antennas for uplink massive MIMO systems. IEEE Trans Commun, 2019, 67: 6829–6843.

2) Yoo I, Smith D R. Dynamic metasurface antennas for higher-order MIMO systems in indoor environments. IEEE Wireless Commun Lett, 2020, 9: 1129–1132.

3) Shlezinger N, Alexandropoulos G C, Imani M F, et al. Dynamic metasurface antennas for 6G extreme massive MIMO communications. IEEE Wireless Commun, 2021, 28: 106–113.

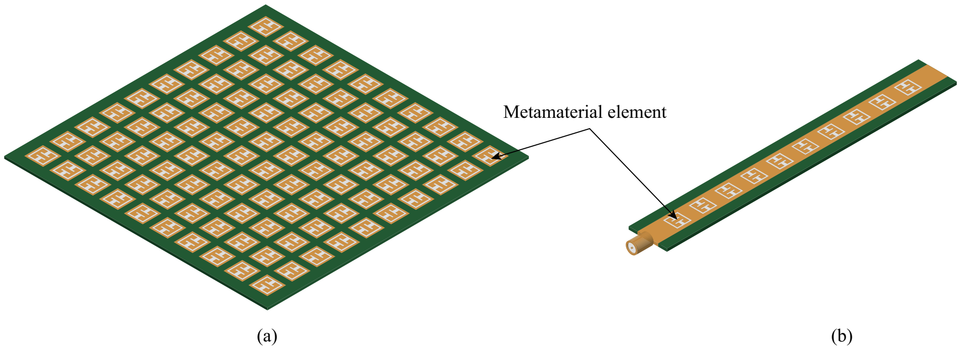

Figure A1 (Color online) Two DMA structures. (a) Two-dimensional planar; (b) one-dimensional microstrip.

$\boldsymbol{h}_{\text{out}} = [h_{\text{out}1}, \ldots, h_{\text{out}I}]^{\mathrm{T}}$, so that the overall channel is the cascade of three parts, that is

$$\boldsymbol{h}_{\text{out}}^{\mathrm{T}} \begin{bmatrix} v_1^{(k)} & & \\ & \ddots & \\ & & v_I^{(k)} \end{bmatrix} \boldsymbol{A\alpha} = \begin{bmatrix} v_1^{(k)} & \cdots & v_I^{(k)} \end{bmatrix} \begin{bmatrix} h_{\text{out}1} & & \\ & \ddots & \\ & & h_{\text{out}I} \end{bmatrix} \boldsymbol{A\alpha} = \left(\boldsymbol{v}^{(k)}\right)^{\mathrm{T}} \boldsymbol{B}, \tag{A2}$$

where $\boldsymbol{B}$ is the cascaded channel of source-to-RIS part and RIS-to-RF-channel part. After changing the RIS pattern K times, an equivalent multi-antenna receive channel can be formed, i.e., $\boldsymbol{V}^{\mathrm{T}}\boldsymbol{B}$, $\boldsymbol{V} = [\boldsymbol{v}^{(1)}, \ldots, \boldsymbol{v}^{(K)}]^{\mathrm{T}}$, which matches the model in (34). In particular, when the receiving antenna is placed at the normal of the RIS and satisfies the far-field condition, then $h_{\text{out}1} = \cdots = h_{\text{out}I}$, the effect of the channel from the RIS to the RF channel can be excluded.

Appendix A.2 Dynamic metasurface antenna

Common DMA structures are shown in Figure A1 and can be described as waveguides in a one-dimensional microstrip or a two-dimensional planar [23]. Similar to the space-fed metasurface antenna, the metamaterial elements can modulate the incident signals' amplitude, phase, and other parameters. Because of the different distances of the metamaterial elements on the antenna to the RF channel, there will be different delays.

For narrowband signals, the delay can be equated to the phase difference. As an example, in the one-dimensional form of DMA, the spacing of the elements is d, and the distance between the ith cell and the RF channel is $(i-1)d$, so the received signal delay is

$$\Delta t_i = \frac{(i-1)d}{\mathrm{c}}, \tag{A3}$$

where c is the light speed. Thus, the relative phase is

$$\Delta\theta_i = 2\pi f \Delta t_i = \frac{2\pi(i-1)d}{\lambda}. \tag{A4}$$

The channel can also be seen as a cascade of three parts: source to DMA, weights of DMA, and elements to RF channel. As the following:

$$\begin{bmatrix} 1 & \cdots & \mathrm{e}^{\mathrm{j}\frac{2\pi(I-1)d}{\lambda}} \end{bmatrix} \begin{bmatrix} v_1^{(k)} & & \\ & \ddots & \\ & & v_I^{(k)} \end{bmatrix} \boldsymbol{A\alpha} = \begin{bmatrix} v_1^{(k)} & \cdots & v_I^{(k)} \end{bmatrix} \begin{bmatrix} 1 & & \\ & \ddots & \\ & & \mathrm{e}^{\mathrm{j}\frac{2\pi(I-1)d}{\lambda}} \end{bmatrix} \boldsymbol{A\alpha} = \left(\boldsymbol{v}^{(k)}\right)^{\mathrm{T}} \boldsymbol{B}. \tag{A5}$$

It can be seen that (A5) and (A2) obtain the same results, and both satisfy the model in (34). Therefore, unlike conventional arrays that improve spatial multiplexing/demultiplexing capability by increasing the number of antennas, using time isomerism, a single metasurface antenna can make the channel equivalent to a conventional multi-antenna channel, enabling multi-stream signals processing. The SPATIO arrays can be constructed with different types of metasurface antennas, thus increasing the effective DOF.